

Monte Carlo calculation of the de-excitation of fission fragments of $^{252}\text{Cf}(\text{sf})$ within multimodal random neck rupture model

Z. Büyükmumcu^{1,2,*} and M. Kildir²

¹*Department of Chemistry, Erciyes University, 38039 Kayseri, Turkey*

²*Department of Chemistry, Middle East Technical University, 06531 Ankara, Turkey*

(Received 20 March 2006; published 29 November 2006)

The multimodal random neck rupture model has been employed to study the energy distribution in nuclear fission. Monte Carlo calculations have been carried out on the de-excitation of fission fragments of $^{252}\text{Cf}(\text{sf})$ using this model. In this study special attention has been paid to the law of conservation of energy. Results for the neutron multiplicities and kinetic energies, average gamma energies are in good agreement with the experimental data. Mass and charge distributions of secondary fission fragments are also well reproduced in the calculations.

DOI: [10.1103/PhysRevC.74.054613](https://doi.org/10.1103/PhysRevC.74.054613)

PACS number(s): 24.75.+i, 25.85.Ca, 24.10.Lx

I. INTRODUCTION

An important question in fission is the partition of the total available energy between complementary fission fragments. There are several models in the literature that deal with the energy partition problem in fission [1–4].

The measured saw-tooth structure of neutron multiplicities, as a function of fragment mass, cannot be understood in the context of the liquid drop model of fission. The small value of average neutron multiplicity for the fragments containing protons and/or neutrons near the magic numbers imply that the shell effects may be important in understanding the saw-tooth structure. In a model proposed by Terrell [1], the fissioning system is assumed to be two spheroidal fragments touching each other at one point at the scission. The deformation-dependent part of the potential has been minimized, leading to a simple expression for describing energy partition between fragments. An important parameter is the stiffness parameter which is influenced strongly by the shell effect. Nuclei near the closed shell structure are resistant against deformation and consequently less deformed than their complementary fragments. Kildir *et al.* [3] proposes an empirical correlation between the stiffness parameter, C_2 , and the shell correction energy, $\delta\omega$, to distribute deformation energy between primary complementary fission fragments for $^{252}\text{Cf}(\text{sf})$. Their results are in good agreement with experimental data. This correlation is further successfully applied to several other fissioning systems [5–7].

The static scission point model proposed by Wilkins *et al.* [2] is good at explaining most of the fission characteristics. This model is based on the assumption of statistical equilibrium among the collective degree of freedom of a system of two nearly touching coaxial spheroids with quadrupole deformations at the scission point. The scission-point configuration from the model provides an interpretation of the saw-tooth neutron emission curve in terms of shell correction related fragment deformations.

Brosa, Grossman, and Müller propose a model (BGM model) in which the assumption of statistical equilibrium

at scission is rejected [4]. The BGM model is a synthesis of two models; random-neck-rupture and multimodal fission. The first model accounts for a fissioning nucleus with a rather long neck connecting the two nascent fragment volumes. The neck cut-up is chosen randomly. This approach, including Rayleigh's instability criterion, describes experimentally observable averages. The experimental distributions in A and TKE can be obtained with high accuracy within the multimodal fission with the random neck rupture model. Several fissioning systems are examined within the BGM model in various other studies [8–10].

In the recent studies [11], The Monte Carlo method is used to study the sequential prompt neutron emission from primary fission fragments. Here, the energy partition between two newborn fragment pairs is calculated in two different ways. In the first approach; identical temperatures are assumed for the complementary fragments. However, the result of the calculations fails to explain the average neutron multiplicity as a function of mass. In the second method, the energy partition is obtained using the experimental neutron multiplicity, neutron energy and gamma energy as a function of mass.

The main purpose of this study was to examine the energy partition in $^{252}\text{Cf}(\text{sf})$ performing some revisions within the multimodal random neck rupture model. In this study, special attention was paid to the conservation of energy which was overlooked in the previous studies [4,12]. In a few studies [9,10], the conservation of energy is considered, in a limited way, so that the calculations are carried out only for the most probable charge of each fragment mass to obtain the averages of various observable quantities. In order to take into account the conservation of energy, the charge distribution should be considered. In this study, empirical parameters determined within the Wahl Z_p model [13] were used to calculate the probability of each charge for a particular mass. Isobars higher than 10^{-6} fractional yields have been used for calculations. Therefore, all isotopes formed with appreciable yields in fission were considered in our study.

After the partition of total available energy between binary-fission fragments using the BGM model, the Monte Carlo method is used to calculate the neutron and gamma-ray emission from fission fragments. The average energy and

*Corresponding author.

number of prompt neutrons and gamma rays are obtained as a function of charge and mass of the primary fission fragments. In addition, neutron multiplicity as a function of kinetic energy is calculated and compared with recent measurements.

II. MODEL ASSUMPTIONS AND CALCULATIONS

A. The multimodal random neck rupture model and determination of pre-scission shapes

According to the BGM model, after leaving the compound or ground state, the nucleus can split into fragments by a number of paths, referred to *modes*. Instead of just one fission barrier in regular fission theories, there are different fission barriers for each mode. A nucleus may have several pre-scission shapes which are distinguished by their total length and asymmetry depending on the mode followed. These modes are named according to the total length and asymmetry of their pre-scission shape; standard (S), superlong (SL), supershort (SS), and superasymmetric (SA) fission modes [4]. In a recent study, fission mode probabilities as a function of nucleus and excitation energy have been systematized in terms of barrier transmission coefficients and bifurcation ratio [14].

In the BGM model, the fissioning nucleus of the semilength l is represented by two spherical heads of the radii of r_1 and r_2 connected by a thick neck at the pre-scission point. A schematic view of the pre-scission shape is given in Fig. 1. The neck radius is r where the neck is thinnest, the thinnest position of the neck is z , the curvature is c , and the extension of the neck is a . The transitional points where two heads are joined to the neck on either side are ζ_1 and ζ_2 . These pre-scission shapes, described by nine parameters, are subject to fluctuations with respect to both the length and asymmetry. When the nucleus stretches beyond the pre-scission shape, the neck snaps randomly because of the *Rayleigh instability*. Even though this process is random, the probability of the rupture at different points of the neck can be estimated.

In our study, three of out of nine parameters, l , r , and c together with the fission mode probabilities are determined from the experimental mass and kinetic energy distribution, the remaining six parameters are determined by solving six equations simultaneously as described by Fan *et al.* [12]. An initial value of l is obtained so that the calculated value of the average total kinetic energy is approximately equal to the experimental one. The neck radius, r , is then estimated using Rayleigh instability criteria:

$$2l = 11r. \quad (1)$$

The parameter, c is related to the width of the mass distribution. It is adjusted throughout the calculation until a

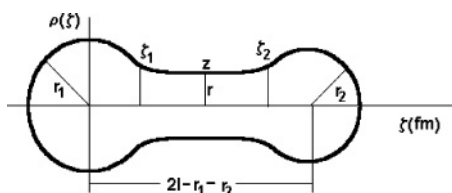


FIG. 1. A schematic view of the pre-scission shape.

value is obtained which produces the experimental width of the mass distribution. Consistency of the calculated values for the average total kinetic energy and the mass distribution, with experimental ones is finally checked to decide on a suitable set of three parameters l , r and c . For every set of three parameters, the remaining six parameters are obtained.

B. Energy balance and energy fractions of fragments

The total energy released in a fission event denoted by Q , is given by the equation

$$Q = \Delta m_{cn} - \Delta m_f - \Delta m_{f,c}, \quad (2)$$

where Δm_{cn} , Δm_f , and $\Delta m_{f,c}$ are the mass excesses of the compound nucleus, the fragment, and its complementary fragment, respectively. Mass excesses were taken from the mass table of Möller *et al.* [15]. Thus total excitation energy of a complementary fragment pair, $E_{exc}(\text{tot})$, is given as

$$E_{exc}(\text{tot}) = Q + E_{cn} - \langle \text{TKE}(A) \rangle, \quad (3)$$

where E_{cn} is the excitation energy of the compound nucleus and $\langle \text{TKE}(A) \rangle$ is the average total kinetic energy for a given mass division. E_{cn} is zero for the spontaneous fission of $^{252}\text{Cf}(\text{sf})$. The total excitation energy for a given complementary primary fragment pair was distributed between two fragments in the form of intrinsic excitation energy and deformation energy. In order to obtain the excitation energy of each fragment, the partition of total excitation energy between complementary fragments needs to be known.

In the original version of the BGM model, the excitation energy of fragments is calculated as a function of mass without paying much attention to the conservation of energy in the fission process. However, energy is conserved on the de-excitation of fission fragments by the evaporation of prompt neutrons and gamma rays. In this study, Eq. (2) and (3) were strictly followed to calculate the total excitation energy of any complementary fragment pair. The average total kinetic energy calculated in the BGM model was subtracted from Q to obtain $E_{exc}(\text{tot})$. We determined the total intrinsic excitation energy, E_s^* , through the nuclear temperature of pre-scission shape of ^{252}Cf within the BGM model. This energy was distributed between complementary fragments proportional to the mass number of each fragment due to its statistical nature. The energy left after subtraction of E_s^* from $E_{exc}(\text{tot})$ was assumed to be equal to the total deformation energy, E_{def}^{tot} , at the scission point:

$$E_{def}^{\text{tot}} = E_{exc}(\text{tot})(Z, A) - E_s^*. \quad (4)$$

We distributed the total deformation energy between complementary fragments to be proportional to the deformations of each fragment. We obtained the following expression for the excitation energy fraction of the fragment in this study:

$$F(Z, A) = \frac{E_{def}^{\text{tot}}(A) \frac{E_{def}(A)}{E_{def}(A) + E_{def}(A_c)} + E_s^* \frac{A}{A_c}}{E_{exc}(\text{tot})}. \quad (5)$$

Here, E_{def} is the deformation energy, A and A_c denotes the mass numbers of a fission fragment and its complementary

partner, respectively. The excitation energy of each fragment is then calculated by the product of $F(Z, A)$ and $E_{\text{exc}}(\text{tot})$.

C. Monte Carlo calculation of prompt neutron and gamma emission

If prompt neutron and gamma emission from fragments are assumed to be a statistical process, the Monte Carlo method proposed by Dostrovsky *et al.* [16] can be used to calculate average number of prompt neutrons emitted and the average energies of prompt neutron and gamma rays. According to this method, the probability of prompt neutron emission from a fragment is given by the equation

$$P_n(\eta)d\eta = \frac{(2s+1)m_n}{\pi^2\hbar^3} \sigma_c \eta \frac{W_2}{W_1} d\eta, \quad (6)$$

where s is the neutron spin, m_n is the mass of neutron, σ_c is the cross section for neutron capture, W_1 is the level density of the nucleus from which the neutron is emitted, W_2 is the level density of the nucleus formed after neutron emission, and η is the kinetic energy of the neutron emitted in the center-of-mass system. Level densities are calculated using the Fermi gas model, which is given by the equation

$$W(E_{\text{exc}}) = C^* \exp[2\sqrt{a'(E_{\text{exc}} - \delta)}], \quad (7)$$

where C is constant and a' is the level density parameter and δ is the pairing correction. The level density parameter strongly depends on the shell structure of the nucleus [17]. In this study, the mass table of Möller *et al.* [15] was used in Eq. (2) to calculate the total energy released in fission. The level density parameter was correlated with the microscopic energies given in that table even though they are not classical shell-corrections, since they include deformation energy. The correlation between the level density parameter and microscopic energy was taken as

$$a' = (0.142A - 2.0 \times 10^{-5} A^2) \times \left[1 + (1 - \exp(-0.051E_{\text{exc}})) \frac{E_{\text{mic}}}{E_{\text{exc}}} \right]. \quad (8)$$

Here E_{mic} is the microscopic energy and the constants in the equation were determined from the best fit of the experimental level density parameters [18]. Figure 2 shows that this general trend is accounted for well by Eq. (8).

The pairing energy, δ is taken to be consistent with the mass table used [15] in which

$$\delta = \delta_p + \delta_n \quad Z \text{ and } N \text{ are even}, \quad (9a)$$

$$\delta = \delta_p \quad Z \text{ is even and } N \text{ is odd}, \quad (9b)$$

$$\delta = \delta_n \quad Z \text{ is odd and } N \text{ is even}, \quad (9c)$$

$$\delta = 0 \quad Z \text{ and } N \text{ are odd}, \quad (9d)$$

$$\delta_p = \frac{4.8B_s}{Z^{1/3}} \quad \text{if } Z \text{ is even}, \quad (9e)$$

$$\delta_n = \frac{4.8B_s}{N^{1/3}} \quad \text{if } N \text{ is even}, \quad (9f)$$

$$B_s = \frac{A^{-2/3}}{4\pi r_0^2} \int_S dS, \quad (9g)$$

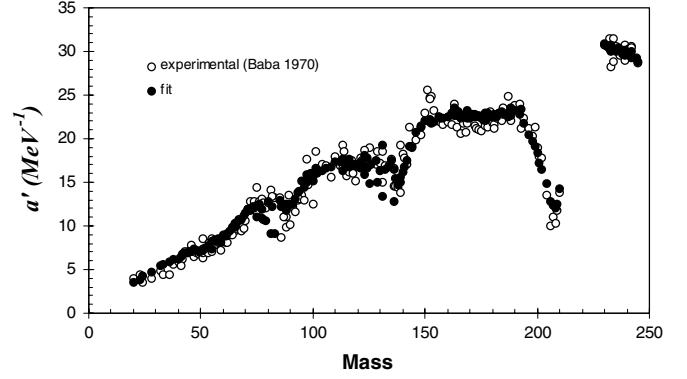


FIG. 2. Experimental [18] and fitted level density parameters as a function of mass.

where δ_p and δ_n are the pairing energies of protons and neutrons, respectively. B_s is the ratio of the surface area of the nucleus of the actual shape to the surface area of the nucleus assuming a spherical shape. It can be calculated exactly at the scission point and at the ground state in our model, since the shape of fragment is known. Since evaporation of neutrons and gamma rays is expected to take place after the fragment has collapsed to its equilibrium shape, B_s is better calculated using the shape parameters of the ground state. Correction for pairing energy in the ground state amounts, at most, to 5% and is neglected in this study; B_s is taken to be 1.0 for every fragment.

A Monte Carlo rejection technique was used in order to select both the excitation energy of a given fragment and the kinetic energy of the emitted neutron. The energy distribution for a primary fragment was assumed to be Gaussian in the range of $E_{\text{exc}} \pm 3\sigma_E$ where σ_E is the width of the kinetic energy distribution for a given mass. After emission of the first neutron, the residual nucleus may have enough excitation energy to evaporate more neutrons. This evaporation process continues until no more neutron emission is possible. After all possible neutrons have been emitted any remaining excitation energy is assumed to be given off in the form of gamma ray. In this calculation, it was assumed that de-excitation of fission fragments by the emission of a neutron is always possible, if its effective excitation energy is larger than the neutron separation energy. Except for the very first step of iteration, only the kinetic energy of the evaporated neutron was selected using the Monte Carlo rejection technique [3]. At the end of each iteration, neutron kinetic energy, the average gamma ray energy and average number of neutrons were weighed by independent yield of the primary fragments for each mass. Fractional independent yields of primary fragments were calculated using Wahl Z_p model [13].

III. RESULTS AND DISCUSSION

A. Pre-scission shapes and average properties of fragments

Parameters of pre-scission shapes have been determined for $^{252}\text{Cf}(\text{sf})$ by Brosa *et al.* [4]. Calculation of potential energy surfaces is carried out by Brosa *et al.* using generalized

TABLE I. The precission shape parameters.

Modes	Standard 1	Standard 2	Standard 3	Superlong
l (fm)	16.60	17.37	19.10	19.50
r (fm)	2.25	2.50	3.47	3.00
c (fm ⁻¹)	1.1×10^{-3}	3.0×10^{-3}	6.9×10^{-3}	2.5×10^{-3}
z (fm)	0.37	0.71	1.50	0.00
r_1 (fm)	6.12	6.14	5.43	5.47
r_2 (fm)	5.78	5.53	4.67	5.47
ζ_1 (fm)	5.15	4.80	2.16	3.27
ζ_B (fm)	16.51	18.95	26.78	24.79
a	0.69	1.07	3.68	1.87

Lawrence shape parametrization with five parameters. They have minimized the potential energy of fissioning system with respect to deformation and found that there are six fission modes for $^{252}\text{Cf}(\text{sf})$. Their shapes are strongly curved therefore yielding a very narrow mass distribution. Fan *et al.* [12] have determined pre-scission shapes using real flat neck representation with nine parameters for other fissioning systems. In these two studies, $r_0 = 1.15$ fm was used to determine pre-scission shapes whereas $r_0 = 1.2249$ fm was used to calculate deformation energy of fission fragments. In this study, we took r_0 as 1.2249 fm for all calculations. Parameters of pre-scission shapes were determined with the procedure outlined in Sec. II A. They are given in Table I. The parameters of pre-scission shapes were obtained excluding supershort and superasymmetric fission modes because of the large errors associated with the experimental results in the mass regions in which these fission modes appear.

The ratio between the l and r values for various fission modes in Table I does not follow Rayleigh instability criteria. It is a fact that the values of l and r obtained from the calculation of potential energy surfaces with Strutinsky shell corrections [4] also disagree with this criteria. Since the Rayleigh instability criteria are derived from the macroscopic properties of a liquid drop, some deviations may be expected when microscopic calculations, including single particle degrees of freedom, are carried out.

SL is the symmetric fission mode with the longest pre-scission shape. The length of standard fission modes (S1, S2, and S3) increase with the average mass of heavy fragments corresponding to that fission mode.

Calculated and experimental mass distributions were compared in Fig. 3. There is an excellent agreement between the two, although there are small discrepancies especially around mass 142. The percent contribution of different fission modes for each mass for two fissioning systems as a function of heavy fragment mass are given in Fig. 4. It is obvious that S3 is the only fission mode that contributes for larger fragment masses. In addition to the SL mode, S3 also contributes to the mass yield around symmetric mass division. This is due to the wide mass distribution of S3. In the other mass regions, two or more fission modes contribute.

The experimental and calculated values of average total kinetic energy as a function of heavy fragment mass were compared in Fig. 5. There is a reasonable agreement between

the experimental and calculated data. The set in Table I was used in the calculations. It may not be the best set since the deformation space may not be exhausted. One of the striking features of the $\langle \text{TKE} \rangle$ distribution is the minimum in the symmetric mass division. This minimum is related mostly to the SL since it has the longest length. As the contribution of the SL mode decreases $\langle \text{TKE}(A) \rangle$ values increase. Depth of minimum is smaller for $^{252}\text{Cf}(\text{sf})$ than that for $^{235}\text{U}(n_{\text{th}}, \text{f})$ [19]. This comes from the fact that SL is the only contributing mode in the symmetric mass region of $^{235}\text{U}(n_{\text{th}}, \text{f})$ whereas there are two contributing modes in the same region of $^{252}\text{Cf}(\text{sf})$. Another reason is the fact that length of SL is not much longer than the lengths of standard modes in the $^{252}\text{Cf}(\text{sf})$.

S1 has the largest contribution to mass yield around $A \approx 130$. It is clear that this is due to the highest kinetic energy values of the S1 mode with the shortest length. Coulomb energy which is the major part of the kinetic energy, decreases as the difference between charges of fragments increases due to the $Z(Z_{\text{cn}} - Z)$ factor in the related equation. This results in a decrease of kinetic energy values with increasing of mass asymmetry in the division.

In order to compare the general trend in neutron multiplicity with that of Brosa *et al.* [4], the total excitation energy in MeV was divided by 8.0, to determine the number of neutrons emitted, from a given primary fission fragment, as in the original BGM model. Although there was no need for this rough approximation, the results were compared with various experiments in Fig. 6. The neutron multiplicity distribution

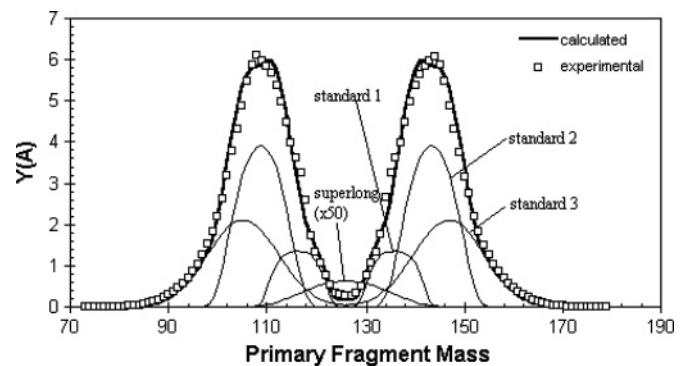


FIG. 3. Comparison of calculated and experimental [22] mass yield distribution for $^{252}\text{Cf}(\text{sf})$.

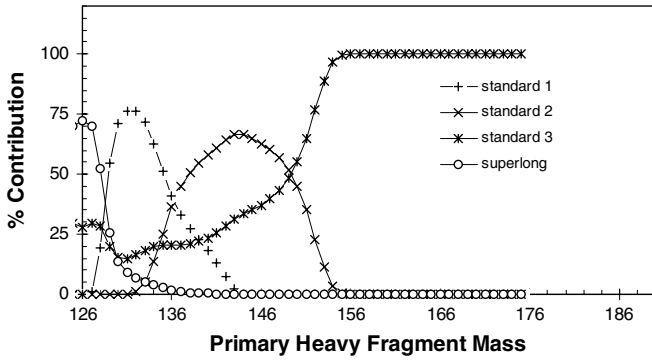


FIG. 4. Percent contribution of each mode as a function of heavy fragment mass for $^{252}\text{Cf}(\text{sf})$.

strongly depends on the mass asymmetry and elongation of the pre-scission shapes, because the deformation energy of a primary fragment at the scission point contributes most to the excitation energy of that fragment. The standard fission modes yield saw-tooth and superlong fission mode yields approximately, linear dependence for the neutron multiplicity as a function of fragment mass (Fig. 7).

An interesting point in Fig. 6 is the appearance of the humps at certain mass numbers. These humps are observed at the mass numbers at which one contributing mode diminishes as another one starts to build up. This effect is due to the fact that the slopes of neutron multiplicity values with respect to mass numbers are different for different fission modes. However, the experimental values of neutron multiplicity seem to have fewer humps than predicted by the BGM model. This means that there may be a smaller number of fission modes than expected from theoretical prediction and/or slopes of the neutron multiplicity curves are approximately equal. However the Monte Carlo method used in this study was a more appropriate tool for the comparison between experiment and calculation since the calculations take into account energy conservation, in addition to the binding energies of emitted neutrons. The neutron multiplicity distribution in this study is in better agreement with experimental values, than that of Brosa *et al.* [4].

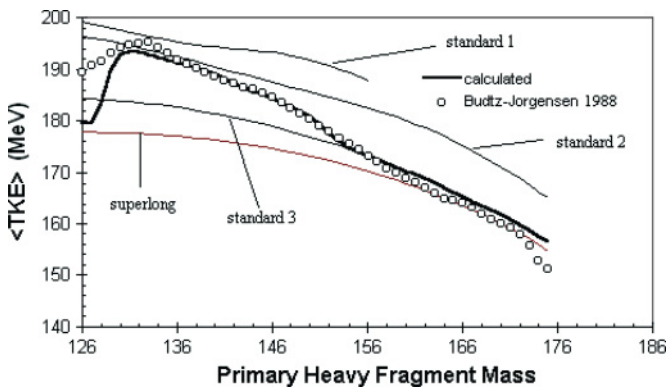


FIG. 5. (Color online) Comparison of calculated and experimental values of average total kinetic energy as a function of heavy fragment mass for $^{252}\text{Cf}(\text{sf})$.

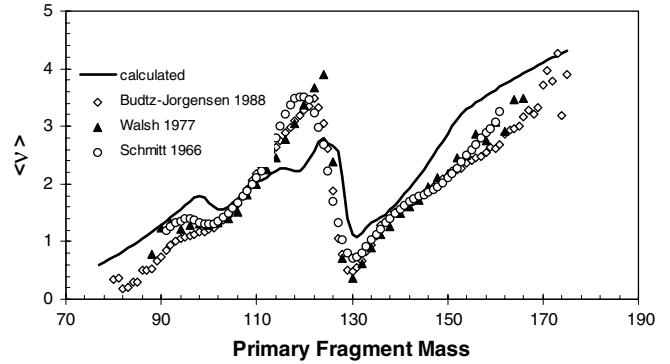


FIG. 6. Comparison of experimental and calculated (BGM recipe) average neutron multiplicities as a function of fragment mass for $^{252}\text{Cf}(\text{sf})$.

The values of fission mode probability, P , average fission fragment mass, $\langle A \rangle$, width of the fragment mass distribution, σ_A , average kinetic energy, $\langle \text{TKE} \rangle$, and average number of neutrons, $\langle \nu \rangle$, for each mode in this study were compared to those of Brosa *et al.* [4] in Table II. It is seen that the superlong fission mode probability is very small with respect to that of standard modes. This low yield of the superlong mode may be due to the higher barrier at the outer saddle point for the superlong mode than that of standard modes.

A correlation can be seen between σ_A and the semilength, l , of the fission mode. As the semilength for a given fission mode increases the width of the fragment mass distribution for that fission mode increases. If the ratio between l and r is kept constant (fixed to the Rayleigh criteria), the neck between the heads becomes more flat with a longer semilength. This results in a higher σ_A value.

Average total kinetic energies are also given for different fission modes of the fissioning system. The lion's share of the total kinetic energy of the fragments comes from the Coulomb repulsion that is inversely proportional to the semi-length of the pre-scission shape. Even though there is a small correction term to account the ellipsoidal deformation of fragments, the total kinetic energy for a given mode decreases as the semilength increases as seen in Tables I and II.

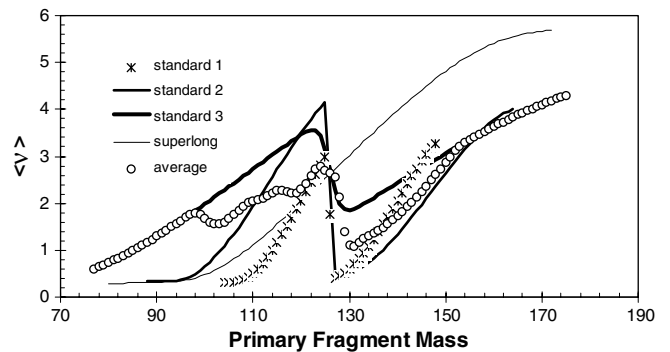


FIG. 7. The decomposition of the calculated values of average neutron multiplicities (BGM recipe) with respect to fission modes for $^{252}\text{Cf}(\text{sf})$.

TABLE II. Comparison of several calculated quantities in this study with the other studies.

	Author	S1	S2	S3	SL	Average
P	this study	14.45	46.60	37.81	1.22	–
	Brosa 1990	8.5	62.0	27.7	1.3	–
$\langle A \rangle$	this study	135.8	143.3	146.8	126.0	–
	Brosa 1990	137	147	–	128	–
σ_A	this study	3.5	4.1	7.1	7.2	–
	Brosa 1990	4.6	6.1	–	13.2	–
$\langle \text{TKE} \rangle$	this study	195.5	188.9	178.1	177.5	185.6
	Brosa 1990	205	194	–	173	–
$\langle \nu \rangle$	this study	2.8	3.5	5.23	5.25	4.1
	Brosa 1990	2.5	3.5	–	6.5	–

In the BGM model, more elongated pre-scission shapes produce more deformed newborn fragments. The number of neutrons emitted from each fission mode is then directly related to the semilength of its pre-scission shape. This relationship is seen in Tables I–III. As a result, $\langle \nu \rangle$ is weakly but inversely correlated with $\langle \text{TKE} \rangle$. The larger value of r_0 used in this study gave lower eccentricity for newborn fragments and the calculated value of $\langle \nu \rangle$ was in better agreement with the experimental value. Since there is no calculation for a fission mode (S3) of this system by Brosa *et al.* [4], a comparison could not be made.

B. Energy distribution between fragments considering energy conservation within the BGM model

In the original version of the BGM model [4], excitation energy of fragments as a function of mass is calculated without paying much attention to the conservation of energy in the process. However, it is essential to conserve energy when performing reasonable calculations of prompt neutron, gamma energy, neutron energy, etc. In order to make sure the energy is conserved in our procedure, we firstly fixed $\langle \text{TKE}(A) \rangle$ values to those calculated within the BGM model. The total excitation energy of complementary fragments was assumed to be equal to the energy obtained when $\langle \text{TKE}(A) \rangle$ was subtracted from the total energy released. Naturally, the total excitation energy of complementary fragments with the same mass number was obtained differently because of the difference in kinetic energy values of different fission modes. The total energy release (sum of Q and compound nucleus excitation) and $\langle \text{TKE}(A) \rangle$ values for different fission modes are given in Fig. 8. Total energy

release is independent of the fission modes since it depends only on the initial and final states of the fissioning nucleus. The total energy release calculated using Eq. (3), taking $E_{cn} = 0$, shows a maximum around the symmetric division. This is due to the fact that extra stable fragments, containing the neutron and proton numbers equal or close to the magic numbers of 82 for neutron and 50 for proton, are produced in this mass region. As a result, more energy is released in this mass region compared to others.

Although total excitation energy as a function of mass and fission modes may be seen from the Fig. 8, they are given in Fig. 9 so the variations can be seen more clearly. The mass dependence of total excitation energy, $E_{\text{exc}}(\text{tot})$ for the different fission modes are similar because of the similar trends in the mass dependence of their kinetic energies. The magnitudes of the total excitation energy are quite different for different fission modes. The SL mode has the highest $E_{\text{exc}}(\text{tot})$ value because it has the most elongated shape and the smallest kinetic energy. On the other hand the smallest $E_{\text{exc}}(\text{tot})$ is S1 fission mode. As a result, Monte Carlo calculations are expected to yield the largest and the smallest values of neutron multiplicities for SL and S1 fission modes, respectively. The average neutron multiplicity for a given fragment mass, $\langle \nu(A) \rangle$ also depends strongly on the contribution of each fission mode due to the averaging process.

Isobaric yields, calculated with the nuclear temperature derived from the intrinsic excitation energy of compound nucleus given by BGM model, are in excellent agreement with experiment as seen in Fig. 3. Therefore, we fixed the intrinsic excitation energy as calculated from BGM model and the remaining energy was assumed to be the total deformation energy of both complementary fragments.

TABLE III. Calculated and experimental average neutron multiplicity values for different modes.

	S1	S2	S3	SL	Average
BGM recipe	2.80	3.54	5.23	5.25	4.09
BGM (Monte Carlo)	3.58	3.46	4.43	5.73	3.87
Brosa 1990	2.5	3.5	–	6.5	–
Aarle 1994 (exp.)	3.8 ± 0.2	3.5 ± 0.4	3.9 ± 0.3	4.2 ± 0.3	–
Axton 1985 (exp.)	–	–	–	–	3.77
Kildir 1982	–	–	–	–	3.68

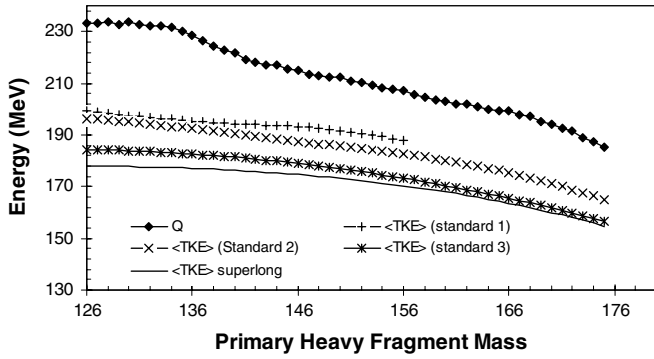


FIG. 8. The weighted average total energy release (Q) and kinetic energy for different fission modes in $^{252}\text{Cf}(\text{sf})$.

Hence, the difference between $E_{\text{exc}}(\text{tot})$ and E_s^* , is distributed between complementary fission fragments according to their deformations in the BGM model.

The excitation energy ratios of the light fragments to the heavy fragments, as a function of heavy fragment mass, are given in Fig. 10, for each mode. We assumed that the intrinsic excitation energy was distributed proportionally to the mass of newborn fragment. This is a natural result of the assumption that nuclear temperature is the same for all parts of the fissioning nucleus at the pre-scission point. On the other hand, the distribution of the deformation energy should depend on the degree of mass asymmetry and radius of the neck. The difference between the number of nucleons on two heads and number of nucleons on the neck region should affect the deformation of the fragment. Generally, the fragments with the same mass ratio may be formed at two rupture points on the neck. But the heavy fragment was formed with the larger probability containing the head with higher number of nucleons. As a result, the neck rupture probability with a relatively higher deformed heavy fragment is generally negligible. This results in the sharp transitions from the light mass region to the heavy mass region in the $\langle \nu \rangle$ values of the standard modes (Fig. 7). But there is slightly smooth transition in the same region of S3 mode due to the relatively long pre-scission shape with long neck. In the symmetric mass divisions of each fission mode, the ratio of the excitation energies of complementary fragments is equal

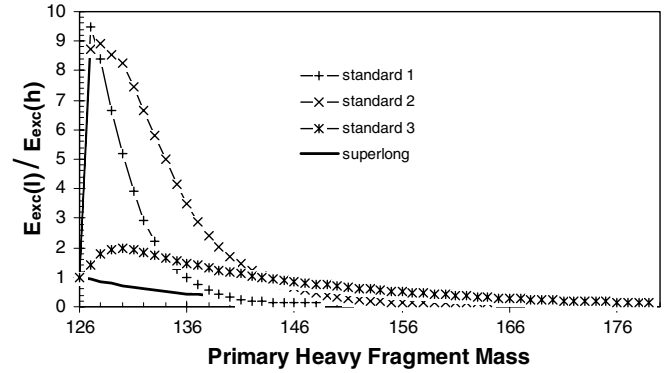


FIG. 10. The ratio of the excitation energy of light fission fragment to that of heavy fragment as a function of heavy fragment mass for $^{252}\text{Cf}(\text{sf})$ in the BGM model.

to one. In the symmetric SL fission mode, this ratio is one because of the equality in mass and deformation for the complementary fission fragments. On the other hand, in the symmetric division of standard fission modes, this ratio is still one since the complementary fragments with the same mass but quite different deformations have exactly the same probability to be formed.

The energy ratio values of the S1 and S2 modes have a sharp increase and decrease, relative to the other modes due to their thinner necks. A thin neck contains smaller mass per unit length of the neck and gives a higher slope of the deformation energies with respect to mass. The resulting neutron multiplicity distribution can be seen in Fig. 6. There is gradual decrease in these ratios for the SL fission mode because of its symmetric pre-scission shape.

C. Results of Monte Carlo calculation

Monte Carlo calculations were carried out to treat de-excitation of fission fragments emitting prompt neutrons and gamma rays. 250 iterations were performed for all isobars having primary fractional yields larger than 10^{-6} . The excitation energy of each isobar was selected in the range $E_{\text{exc}} \pm 3\sigma_E$ for each iteration.

The experimental and calculated values of average prompt neutron multiplicities as a function of fragment mass were compared in Fig. 11. Our calculations produced the experimentally known saw-tooth structure of neutron multiplicities. There is good agreement between the calculated and experimental values as seen in Fig. 11.

There are some differences between the results of Monte Carlo calculations within the BGM model (MC-BGM) and calculations with the simple-BGM model as seen in Fig. 12. The differences are mainly due to the energy conservation was used in the MC-BGM.

MC-BGM gives larger values of $\langle \nu(A) \rangle$ in the region at which S1 is the dominant mode. Average neutron multiplicity value of simple-BGM is less than that of MC-BGM (Table III). This is mainly due to the $Z = 50$ and $N = 82$ spherical shells. The deformation energy calculated macroscopically within the BGM model does not take into account shell and pairing

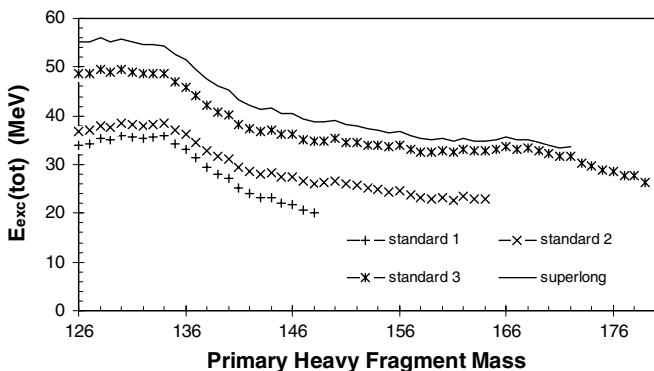


FIG. 9. The sum of the excitation energies of complementary fragments as a function of heavy fragment mass for $^{252}\text{Cf}(\text{sf})$.

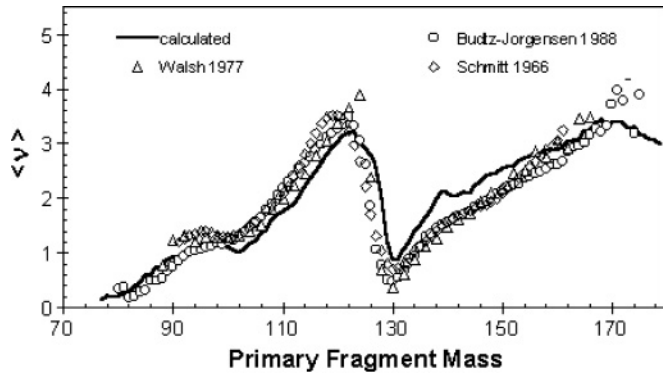


FIG. 11. Comparison of experimental and calculated (MC-BGM) average neutron multiplicities as a function of fragment mass for $^{252}\text{Cf}(\text{sf})$.

corrections. When closed-shell fragments are formed in fission, more energy will be released compared to that of the formation of midshell fragments. This effect is taken into account in MC-BGM through the calculation of total energy release using the mass equation. It is obvious that MC-BGM gives better agreement with the experiment data [20] (Table III). It is interesting that the experimental value of $\langle \nu(A) \rangle$ for S2 is less than that for S1 (Table III) although the pre-scission shape of S2 is longer than that of S1 resulting in a lower $\langle \text{TKE}(A) \rangle$ in S2. This may be more evidence for the shell effect stated above. Another interesting point is the decrease in the average neutron multiplicities after some mass asymmetry although deformations increase gradually with mass. This can be attributed to the change in available excitation energy as a result of a change in the deformation of fragment as a function of mass asymmetry.

Another interesting feature is the agreement of the results of MC-BGM for the masses between 110–124, in spite of the disagreement of results estimated from the simple-BGM. In this region, some humps in simple-BGM were not seen in MC-BGM. This shows that the excitation energy available in this region is higher than that of simple-BGM. The higher energy than expected from the pre-scission shapes could also be attributed to the $Z = 50$ shell effect as stated in the previous paragraph. It should be stressed that the deformation

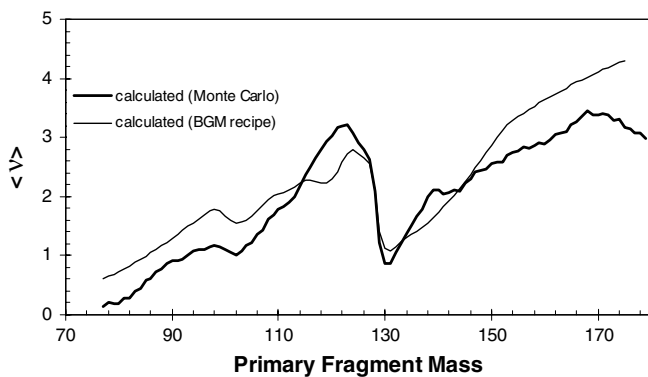


FIG. 12. Comparison of calculated values of average neutron multiplicities by Monte Carlo method and BGM recipe [4] within the BGM model for $^{252}\text{Cf}(\text{sf})$.

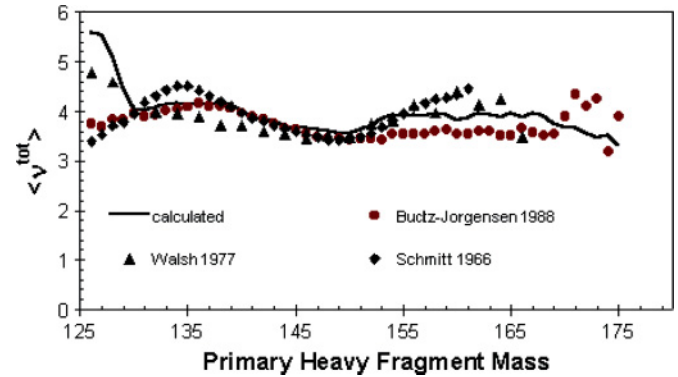


FIG. 13. (Color online) Comparison of experimental and calculated values of total neutron multiplicity as a function of fragment mass for $^{252}\text{Cf}(\text{sf})$.

energy was fixed by the ratio obtained from the pre-scission shapes. This can be seen clearly in the MC-BGM results, in such cases higher neutron multiplicity was obtained for both complementary fragments. It may be noted that the higher neutron multiplicity depends also on the binding energies of each emitted neutron which vary with mass and charge of the fragment. Another interesting result of BGM model in the Fig. 11 is the lower neutron multiplicity values with respect to experimental values in the light fragments. The reverse trend is observed for the heavy fragments. MC-BGM results are in good agreement with observed experiments. This is mainly due to the better fit of the $\langle \text{TKE} \rangle$ values in the regions in which most of the fragment yields appear. Average neutron multiplicities for different calculations are compared with the experimental values in Table III.

The calculated values of the sum of the neutron multiplicities of complementary fragments as a function of heavy fragment mass are compared with the experimental values in Fig. 13. The total neutron multiplicity is not the same for each division and there is a maximum in the symmetric mass division. There is a reasonable agreement between the results of the calculation and experimental values. The sizable differences between the various experimental results are noticeable around the symmetric mass division.

Average prompt neutron multiplicity as a function of fragment charge is given in Fig. 14. The general trend, here, is

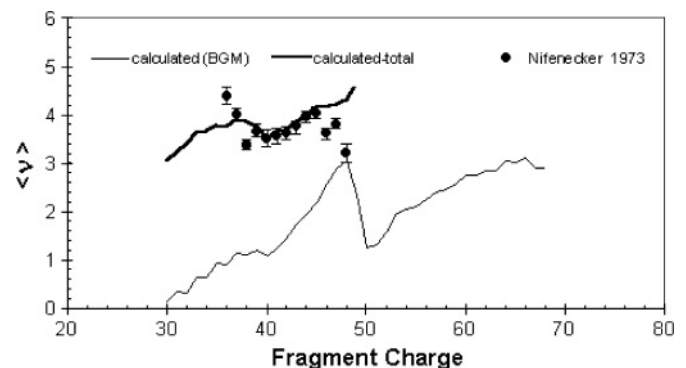


FIG. 14. Comparison of experimental and calculated prompt neutron multiplicity as a function of fragment charge for $^{252}\text{Cf}(\text{sf})$.

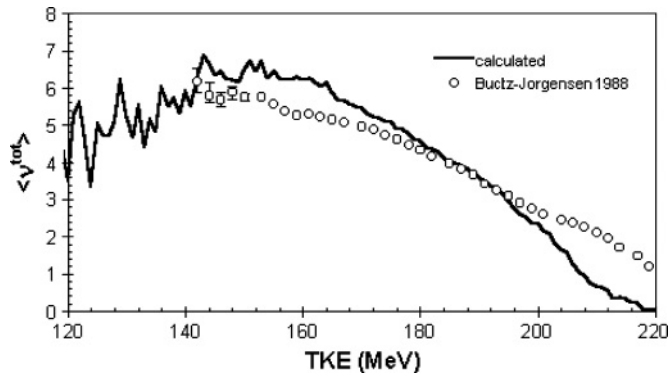


FIG. 15. Comparison of the experimental and calculated total neutron multiplicity as a function of total kinetic energy for $^{252}\text{Cf}(\text{sf})$.

very similar to that of the average prompt neutron multiplicity as a function of fragment mass, since the charge of the fragment is proportional to the mass of the fragment with a small deviation due to charge polarization.

It is clear that the formation of even- Z complementary fragment results in excess energy release because of the pairing term in the mass equation. This excess energy is approximately 2 MeV for even- Z fissioning nuclei. The odd-even effect is not seen in the average prompt neutron emitted as a function of Z . It may be because this energy either appears in the form of kinetic energy in fragments and/or the energy is dissipated as gamma rays. Experimental values of neutron multiplicity as a function of Z are available for $^{252}\text{Cf}(\text{sf})$ [21]. Although there is a small discrepancy near the asymmetric and symmetric regions, there is a good agreement between experimental and calculated values.

The variation of average number of neutrons as a function of total kinetic energy (TKE) is compared in Fig. 15. Below $\text{TKE} \approx 160$ MeV, the total average prompt neutron multiplicity sharply deviates from the linear dependence observed by Ref. [22]. An increase in total average neutron multiplicity, $\langle \nu^{tot} \rangle$, is expected with a decrease in TKE, because more of the energy released in fission would be available as excitation energy of the fragments as observed by Lemaire *et al.* [11]. Nishio *et al.* [23] stated that the physical explanation of nonlinear behaviour of $\langle \nu^{tot} \rangle$ below $\text{TKE} \approx 160$ MeV is not clear. We may offer an explanation of this behavior within the framework of BGM with the aid of Figs. 4 and 9. The more compact fission modes of S1 and S2 are dominant in the mass region of 102–150, contributing to the high TKE portion of the neutron spectra in Fig. 15. The average total excitation energy of complementary fragments reaches a maximum at about 40 MeV. In this region, an increase in total average neutron multiplicity, $\langle \nu^{tot} \rangle$, is expected with a decrease in TKE, because more of the energy released in fission would be available as excitation energy of fragments, for each of the S1 and S2 modes. On the other hand, the more elongated fission mode of S3 becomes dominant outside of the 102–150 mass region which contributes to the low TKE portion of the neutron spectra. The average total excitation energy of complementary fragments is about 28 to 34 MeV. In this mass region, fragments with low $\langle \text{TKE} \rangle$ values also have lower excitation energies because of the corresponding decrease in

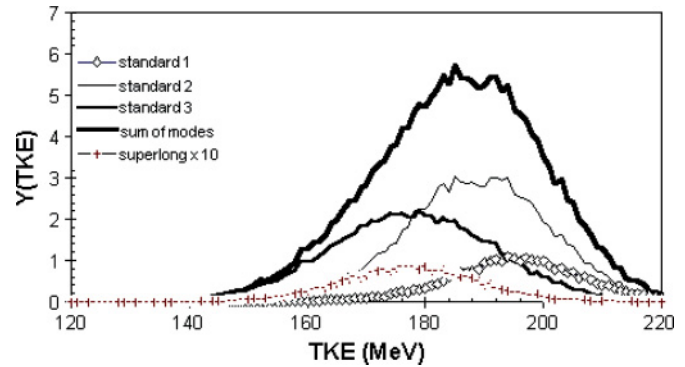


FIG. 16. (Color online) Calculated relative yield distribution of total kinetic energies for different fission modes of $^{252}\text{Cf}(\text{sf})$.

the total energy released [19]. Therefore, we expect a linear increase in total neutron multiplicity at high TKE values and it reaches a maximum and even decreases, somewhat, at lower TKE values due to the contribution of the S3 mode. Hence a deviation from linearity is expected. Although calculated values from this study do not show a good quantitative agreement with experimental results, there is good qualitative agreement showing deviation from linearity and a positive slope. Poor quantitative agreement in the results mostly comes from the disagreement between calculated and experimental $\langle \text{TKE} \rangle$ values. As stated previously, initial excitation energy was selected by the Monte Carlo rejection technique at the start of each iteration. Total kinetic energy values for each iteration are obtained by subtracting selected total excitation energy from total energy release ($Q + E_{cn}$). The distribution of kinetic energies is given in Fig. 16. These distributions are found to be Gaussian, because the excitation energy for each iteration was chosen from a Gaussian distribution using the Monte Carlo rejection technique.

Since we assumed that the gamma ray emission does not occur when it is energetically possible to emit neutrons, fragments dissipate their remaining excitation energies in the form of gamma rays after neutron emission. Average gamma energies as a function of fragment mass are compared in Fig. 17. There is a fine structure due to an odd-even effect. The calculated values are generally higher than the experimental ones. The fine structure due to the odd-even effect is observed

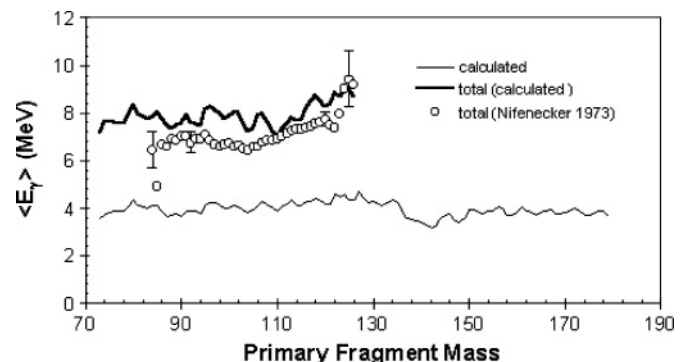


FIG. 17. Comparison of calculated and experimental average gamma energies as a function of fragment mass for $^{252}\text{Cf}(\text{sf})$.

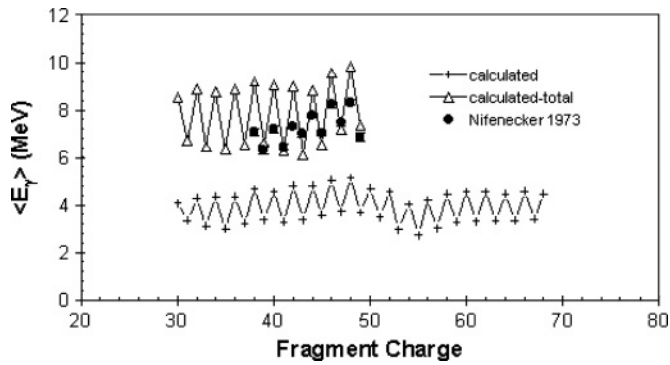


FIG. 18. Comparison of calculated and experimental average gamma ray energies as a function of fragment charge for $^{252}\text{Cf}(\text{sf})$.

both in calculated and experimental results indicating a fairly good agreement between the two. The excitation energy remaining for gamma emission in the secondary fission fragment would be between zero and the energy needed to emit neutron (binding energy + kinetic energy of the emitted neutron). Thus each fragment would have average excitation energy equal to about half of the energy needed to emit neutron, to be dissipated as gamma rays.

Average gamma energies as a function of fragment charge are given in Fig. 18. Experimental values for the total gamma energies as a function of light fragment mass are available for comparison with calculated values. It is seen that the fine structure in experimental results is reproduced, but with a larger magnitudes, in the calculations. Similar results are obtained in another study for the same system [3,24]. As stated by Kildir [24], this may be mostly due to the assumption of the constant TKE value for all the isobars of the mass chain. The odd-even effect is observed experimentally in the same system [21]. From such an interpretation it can be said that extra energy release in the formation of even-even fragments appears in the both total kinetic kinetic energy of fragments and the energies of gamma rays.

The change of mass in fragments due to the emission of neutrons produces a change in the mass yields. The mass yield is decreased due to the decrease of the mass number by the number of neutrons emitted from the fragment. At the same time, the yield of the same mass is increased due to neutron emission from higher mass fragments resulting in formation of product with that mass. The experimental and calculated values of primary and secondary mass yields are compared in Fig. 19. There is a shift in the secondary yield distribution to the lighter mass and a large difference between primary and secondary yields near the symmetric region. This is because a fragment emits a large number of neutrons in this mass region while its complementary fragment with a little higher mass emits a small number of neutrons. There is a good agreement between calculated and the experiment based systematics [13] secondary yields as seen in Fig. 19.

Charge to mass ratio (Z/A) of fragments deviates from that of the fissioning nucleus. Since the charge of all isobars are not the same because of motion of both protons and neutrons through the fissioning nucleus at the pre-scission point. At the time of rupture, there is some probability for

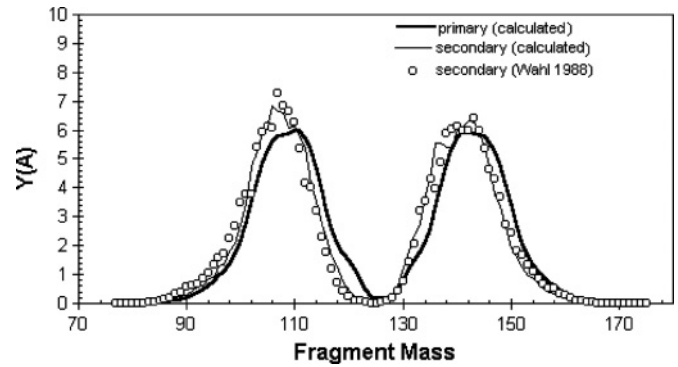


FIG. 19. Calculated primary and calculated and experimental (evaluated [13]) secondary mass yield distribution for $^{252}\text{Cf}(\text{sf})$.

the existence of any nucleon of the fissioning system at any part of the system. This results in distribution of charge for isobars rather than having a unique value of charge. This distribution may be assumed to be Gaussian with constant width which is particular for each fissioning system [13]. The width parameters for primary and secondary yields are shown in Fig. 20. Isobaric charge distribution widths, σ_z of secondary yields are calculated after Monte Carlo calculations of prompt neutron emission in the same code. It is clearly seen that the widths of secondary yield distributions are higher than that of primary yields. This is because the charge range of the mass chain is extended due to neutron evaporation of fragments with the higher mass. If charge density of fragments may be assumed to be approximately the same with that of fissioning system, charge of fragments is directly related to the mass number of fragment. Therefore fragments with the high atomic and mass number produces fragments with the smaller mass number but with the same atomic number due to neutron evaporation. The result is the broadening of the widths of the secondary mass chains with respect to that of the primary. This broadening can easily be seen in Fig. 20.

There is a minimum in the width around $A \approx 130$. This is due to the fact that neutron multiplicity is very low in this mass region and as a result the broadening in the charge distribution is reduced.

The most probable charge for each isobar chain is symbolized as Z_p in the Wahl model [13]. If the charge-to-mass ratio of the fissioning nucleus were preserved in the fragments in

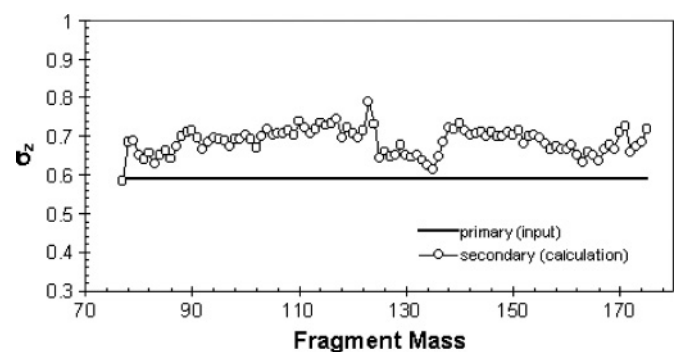


FIG. 20. Widths of charge distribution calculated with BGM model for secondary yields of $^{252}\text{Cf}(\text{sf})$.

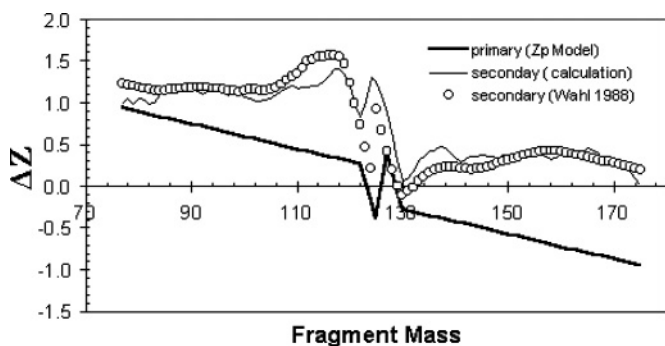


FIG. 21. Comparison of charge polarization, ΔZ of secondary fragments calculated with the BGM and Wahl models in $^{252}\text{Cf}(\text{sf})$

the fission process, the most probable charge can be predicted with the assumption of unchanged charge distribution (Z_{ucd}). The Z_{ucd} can easily be obtained from the product of fragment mass with the charge-to-mass ratio of the fissioning nucleus. Z'_p 's are observed to be slightly different than Z_{ucd} . This phenomenon is called charge polarization and it is denoted by $\Delta Z = Z_p - Z_{\text{ucd}}$. These ΔZ values for primary fragments calculated from the Z_p model of Wahl are shown in Fig. 21. It has a positive value for light fragments and a negative one for heavy fragments. This is related to the ratio of the surface energy to the Coulomb energy of nucleus. At equilibrium, the surface energy balances the Coulomb energy. At this equilibrium, the ratio between these two energies increases as the volume of the nucleus increases. Surface energy and Coulomb energy are proportional to the terms $A^{2/3}$ and $Z^2/A^{1/3}$. Therefore surface-to-Coulomb energy ratio would be proportional to Z^2/A and so the charge density (Z/A) of heavy nuclei is smaller than that of light nucleus to keep Z^2/A constant. Charge polarisation phenomena is the reflection of this fact coming from the surface-to-Coulomb energy ratio differences at different regions of fissioning systems (heavy head, light head and neck region). As a result the charge density of the heavy fragments is smaller than that of light ones. This is clear from the values calculated using the empirical Z_p model of Wahl, which are given in Fig. 21.

The emission of the neutron causes an increase in the charge density of fragments since the mass number decreases by one with no change in their charge. It is clear that this causes an increase in charge polarization values as seen from Fig. 21. This effect results in positive charge polarization values for the most of the secondary heavy fragment region. As seen from Fig. 21, there is a good agreement between the experiment based systematics [13] and calculated values.

IV. CONCLUSION

In conclusion, we have employed a tool to study the emission of neutrons and gamma rays from fission fragments using the Monte Carlo method within the BGM model [4]. The pre-scission shape for each fission mode is determined by employing the experimental mass and kinetic energy distributions in the spontaneous fission of ^{252}Cf . As a result of the good agreement obtained between the calculated and experimental values of several important quantities in the spontaneous fission of ^{252}Cf , it is concluded that the BGM model may be used to study quantitatively, mass, kinetic energy, mode probability and excitation energy distributions of primary fission fragments in the nuclear fission. The sequential emission of neutrons and gamma rays from primary fission fragments is taken as a statistical process and treated by a Monte Carlo method. The mass dependence of the average number of prompt neutrons is shown in Fig. 11. The saw-tooth structure is well reproduced indicating that the partition of excitation energy in the fission process is accounted for well within the BGM model. The total kinetic energy dependence of the total neutron multiplicity shows saturation behavior at lower TKE values, as seen in Fig. 15. Such behavior may be expected as a result of multimodal fission. In the recent study by Lemaire [11] it was concluded that the partition of total excitation energy between light and heavy fragments was treated adequately neither by assuming the fragments have the same temperature nor by using experimental values of emitted neutrons and gamma rays. Failure of equal temperature hypothesis had been concluded also by Kildir [24]. In this paper, we offer a new hypothesis based on the BGM model. Here, the pre-scission shape determined by employing the experimental mass and kinetic energy distributions in a given fissioning system could represent a relatively stable state, which ruptures due to Rayleigh instability, forming two deformed fragments touching each other at the scission point. Computational results obtained on the mass, kinetic energy, neutron and gamma ray multiplicity distributions are directly dependent on the pre-scission shapes. This study will be extended to other fissioning nuclei to investigate the validity of the model.

ACKNOWLEDGMENT

This study is supported by Research Fund of Middle East Technical University (Ankara-Turkey).

- [1] J. Terrell, in *Proceedings of IAEA Symposium On Physics and Chemistry of Fission, Salzburg, 1965*, (IAEA, Vienna), Vol. II, p. 3.
- [2] B. Wilkins, E. Steinberg, and R. Chassman, *Phys. Rev. C* **14**, 1832 (1976).
- [3] M. Kildir and N. K. Aras, *Phys. Rev. C* **25**, 365 (1982).
- [4] U. Brosa, S. Grossman, and A. Müller, *Phys. Rep.* **197**, 167 (1990).
- [5] A. Ruben, H. Märten, and D. Seeliger, *Z. Phys. A* **338**, 67 (1991).
- [6] U. Gohs and H. Marten, in *Nuclear Data for Neutron Emission*

in the Fission Process, edited by S. Ganesan, INDC(NDS)-251 (IAEA Nuclear Data Section, Vienna, 1991).

- [7] Z. Büyükmumcu and M. Kildir, *J. Radioanal. Nucl. Chem.* **220**, 27 (1997).
- [8] T. Ohsawa, T. Horiguchi, and M. Mitsuhashi, *Nucl. Phys.* **A665**, 3 (2000).
- [9] A. Tudora, B. Morillon, F.-J. Hamsch, G. Vladuca, and S. Oberstedt, *Nucl. Phys.* **A756**, 176 (2005).
- [10] F.-J. Hamsch, A. Tudora, G. Vladuca, and S. Oberstedt, *Ann. Nucl. En.* **32**, 1032 (2005).

- [11] S. Lemaire, P. Talou, T. Kawano, M. B. Chadwick, and D. G. Madland, *Phys. Rev. C* **72**, 024601 (2005); **73**, 014602 (2006).
- [12] T. Fan, J. Hu, and S. Bao, *Nucl. Phys.* **A591**, 161 (1995).
- [13] A. C. Wahl, *At. Data Nucl. Data Tables* **39**, 1 (1988).
- [14] U. Brosa, H.-H. Knitter, T. Fan, J. Hu, and S. Bao, *Phys. Rev. C* **59**, 767 (1999).
- [15] P. Möller, J. R. Nix, W. D. Myers, and W. J. Swiatecki, *At. Data Nucl. Data Tables* **59**, 185 (1995).
- [16] I. Dostrovsky, Z. Fraenkel, and G. Friedlander, *Phys. Rev.* **116**, 683 (1959).
- [17] A. V. Ignatyuk, G. N. Smirenkin, and A. S. Tishin, *Sov. J. Nucl. Phys.* **21**, 255 (1975).
- [18] H. Baba, *Nucl. Phys.* **A159**, 625 (1970).
- [19] Z. Büyükmumcu, Ph.D. thesis, Middle East Technical University, 1998.
- [20] J. van Aarle, W. Westmeier, R. A. Esterlund, and P. Patzelt, *Nucl. Phys.* **A578**, 77 (1994).
- [21] H. Nifenecker, C. Signarbieux, R. Babinet, and J. Poitou, in *Proceedings of IAEA Symposium on Physics and Chemistry of Fission*, Rochester, 1973, p. 117.
- [22] C. Budtz-Jorgensen and H.-H. Knitter, *Nucl. Phys.* **A490**, 307 (1988).
- [23] K. Nishio, Y. Nakagome, H. Yamamoto, and I. Kimura, *Nucl. Phys.* **A632**, 540 (1998).
- [24] M. Kildir, Associate Professor thesis, Middle East Technical University, 1978.